First Measurement of the $B \to \pi \ell \nu$ and $B \to \rho(\omega)\ell\nu$ Branching Fractions

J. P. Alexander,[1] C. Bebek,[1] B. E. Berger,[1] K. Berkelman,[1] K. Bloom,[1] D. G. Cassel,[1] H. A. Cho,[1] D. M. Coffman,[1] D. S. Crowcroft,[1] M. Dickson,[1] P. S. Drell,[1] D. J. Dumas,[1] R. Ehrlich,[1] R. Elia,[1] P. Gaidarev,[1] B. Gittelman,[1] S. W. Gray,[1] D. L. Hartill,[1] B. K. Heltsley,[1] C. D. Jones,[1] S. L. Jones,[1] J. Kandaswamy,[1] N. Katayama,[1] P. C. Kim,[1] D. L. Kreinick,[1] T. Lee,[1] Y. Liu,[1] G. S. Ludwig,[1] J. Masui,[1] J. Mevissen,[1] N. B. Mistry,[1] C. R. Ng,[1] E. Nordberg,[1] J. R. Patterson,[1] D. Peterson,[1] D. Riley,[1] A. Soffer,[1] C. Ward,[1] P. Avery,[2] C. Prescott,[2] S. Yang,[2] J. Yelton,[2] G. Brandenburg,[3] R. A. Briere,[3] T. Liu,[3] M. Saulnier,[3] R. Wilson,[3] H. Yamamoto,[3] T. E. Browder,[4] F. Li,[4] J. L. Rodriguez,[4] T. Bergfeld,[5] B. I. Eisenstein,[5] J. Ernst,[5] G. E. Gladding,[5] G. D. Gollin,[5] I. Karliner,[5] M. Palmer,[5] M. Selen,[5] J. J. Thaler,[5] K. W. Edwards,[6] M. Ogg,[6] A. Bellerive,[7] D. I. Britton,[7] R. Janicek,[7] D. B. MacFarlane,[7] K. W. McLean,[7] P. M. Patel,[7] A. J. Sadoff,[8] R. Ammar,[9] P. Baringer,[9] A. Bean,[9] D. Besson,[9] D. Coppage,[9] N. Copty,[9] R. Davis,[9] N. Hancock,[9] S. Kotov,[9] I. Kravchenko,[9] N. Kwak,[9] S. Anderson,[10] Y. Kubota,[10] M. Lattery,[10] J. J. O'Neill,[10] S. Patton,[10] R. Poling,[10] T. Riehle,[10] V. Savinov,[10] A. Smith,[10] M. S. Alam,[11] S. B. Athar,[11] I. J. Kim,[11] Z. Ling,[11] A. H. Mahmood,[11] H. Severini,[11] S. Timm,[11] F. Wappler,[11] J. E. Duboscq,[12] D. Fujino,[12] R. Fulton,[12] K. K. Gan,[12] K. Honscheid,[12] H. Kagan,[12] R. Kass,[12] J. Lee,[12] M. Sung,[12] A. Undrus,[12],* R. Wanke,[12] C. White,[12] A. Wolf,[12] M. M. Zoeller,[12] B. Nemati,[13] S. J. Richichi,[13] W. R. Ross,[13] P. Skubic,[13] M. Wood,[13] M. Bishai,[14] J. Fast,[14] E. Gerndt,[14] J. W. Hinson,[14] D. H. Miller,[14] E. I. Shibata,[14] I. P. J. Shipsey,[14] M. Yurko,[14] M. Battle,[15] L. Gibbons,[15] S. D. Johnson,[15] Y. Kwon,[15] S. Roberts,[15] K. Sparks,[15] E. H. Thorndike,[15] C. P. Jessop,[16] K. Lingel,[16] H. Marsiske,[16] M. L. Perl,[16] S. F. Schaffner,[16] R. Wang,[16] T. E. Coan,[17] V. Fadeyev,[17] I. Korolkov,[17] Y. Maravin,[17] I. Narsky,[17] V. Shelkov,[17] J. Staeck,[17] R. Stroynowski,[17] I. Volobouev,[17] J. Ye,[17] M. Artuso,[18] A. Efimov,[18] M. Gao,[18] M. Goldberg,[18] R. Greene,[18] D. He,[18] S. Kopp,[18] G. C. Moneti,[18] R. Mountain,[18] Y. Mukhin,[18] T. Skwarnicki,[18] S. Stone,[18] X. Xing,[18] J. Bartelt,[19] S. E. Csorna,[19] V. Jain,[19] S. Marka,[19] A. Freyberger,[20] D. Gibaut,[20] K. Kinoshita,[20] I. C. Lai,[20] P. Pomianowski,[20] S. Schrenk,[20] G. Bonvicini,[21] D. Cinabro,[21] B. Barish,[22] M. Chadha,[22] S. Chan,[22] G. Eigen,[22] J. S. Miller,[22] C. O'Grady,[22] M. Schmidtler,[22] J. Urheim,[22] A. J. Weinstein,[22] F. Würthwein,[22] D. M. Asner,[23] M. Athanas,[23] D. W. Bliss,[23] W. S. Brower,[23] G. Masek,[23] H. P. Paar,[23] J. Gronberg,[24] C. M. Korte,[24] R. Kutschke,[24] D. J. Lange,[24] S. Menary,[24] R. J. Morrison,[24] S. Nakanishi,[24] H. N. Nelson,[24] T. K. Nelson,[24] C. Qiao,[24] J. D. Richman,[24] D. Roberts,[24] A. Ryd,[24] H. Tajima,[24] M. S. Witherell,[24] R. Balest,[25] B. H. Behrens,[25] K. Cho,[25] W. T. Ford,[25] M. Lohner,[25] H. Park,[25] P. Rankin,[25] J. Roy,[25] and J. G. Smith[25]

(CLEO Collaboration)

[1]*Cornell University, Ithaca, New York 14853*
[2]*University of Florida, Gainesville, Florida 32611*
[3]*Harvard University, Cambridge, Massachusetts 02138*
[4]*University of Hawaii at Manoa, Honolulu, Hawaii 96822*
[5]*University of Illinois, Champaign-Urbana, Illinois 61801*
[6]*Carleton University and Institute of Particle Physics, Ottawa, Ontario Canada K1S 5B6*
[7]*McGill University and Institute of Particle Physics, Montréal, Québec, Canada H3A 2T8*
[8]*Ithaca College, Ithaca, New York 14850*
[9]*University of Kansas, Lawrence, Kansas 66045*
[10]*University of Minnesota, Minneapolis, Minnesota 55455*
[11]*State University of New York at Albany, Albany, New York 12222*
[12]*The Ohio State University, Columbus, Ohio 43210*
[13]*University of Oklahoma, Norman, Oklahoma 73019*
[14]*Purdue University, West Lafayette, Indiana 47907*
[15]*University of Rochester, Rochester, New York 14627*
[16]*Stanford Linear Accelerator Center, Stanford University, Stanford, California 94309*
[17]*Southern Methodist University, Dallas, Texas 75275*
[18]*Syracuse University, Syracuse, New York 13244*
[19]*Vanderbilt University, Nashville, Tennessee 37235*
[20]*Virginia Polytechnic Institute and State University, Blacksburg, Virginia 24061*
[21]*Wayne State University, Detroit, Michigan 48202*
[22]*California Institute of Technology, Pasadena, California 91125*
[23]*University of California, San Diego, La Jolla, California 92093*
[24]*University of California, Santa Barbara, California 93106*
[25]*University of Colorado, Boulder, Colorado 80309-0390*

CLEO has studied B decays to $\pi\ell\nu$, $\rho\ell\nu$, and $\omega\ell\nu$, where $\ell = e$ or μ, by incorporating the missing momentum into full B reconstruction. With the B^0 and B^+ modes combined according to isospin predictions for the relative partial widths, we obtain $\mathcal{B}(B^0 \to \pi^-\ell^+\nu) = (1.8 \pm 0.4 \pm 0.3 \pm 0.2) \times 10^{-4}$ and $\mathcal{B}(B^0 \to \rho^-\ell^+\nu) = (2.5 \pm 0.4^{+0.5}_{-0.7} \pm 0.5) \times 10^{-4}$, where the errors are statistical, systematic, and the estimated model dependence. We also estimate $|V_{ub}| = (3.3 \pm 0.2^{+0.3}_{-0.4} \pm 0.7) \times 10^{-3}$. [S0031-9007(96)01807-8]

The Cabbibo-Kobayashi-Maskawa matrix [1], which rotates the quark system from the physical to the weak eigenstates, provides a mechanism for *CP* violation. To determine whether the Cabibbo-Kobayashi-Maskawa (CKM) matrix is indeed the source of *CP* violation, it is essential to measure V_{ub}, the CKM element coupling the b and u quarks. A nonzero value for $|V_{ub}|$ has been demonstrated [2,3] at the $\Upsilon(4S)$ by the observation of leptons in a high momentum range accessible to $b \to u\ell\nu$ decays but rarely reached in the dominant $b \to c\ell\nu$ process. The values for $|V_{ub}|$ so obtained have large theoretical uncertainties because the details of hadronization significantly affect the lepton spectrum in this range.

Study of exclusive $b \to u\ell\nu$ channels, where the theoretical challenge is the form factor calculation, provides an alternate route to $|V_{ub}|$. The CLEO experiment at the Cornell Electron Storage Ring (CESR) has set an upper limit [4] in the combined modes $\rho^-\ell^+\nu$, $\rho^0\ell^+\nu$, and $\omega\ell^+\nu$. This Letter presents a new CLEO study of $B^0 \to \pi^-\ell^+\nu$, $B^+ \to \pi^0\ell^+\nu$, $B^0 \to \rho^-\ell^+\nu$, $B^+ \to \rho^0\ell^+\nu$, $B^+ \to \omega\ell^+\nu$, and charge conjugate decays, where $\ell = e$ or μ, in an $\Upsilon(4S)$ data sample of 2.66 fb^{-1} (2.84×10^6 $B\bar{B}$ pairs).

The CLEO detector [5] contains three concentric wire chambers within a 1.5 T superconducting solenoid that detect charged particles over 95% of the solid angle. The momentum resolution at 2 GeV/c is 0.6%. A CsI(Tl) electromagnetic calorimeter, also inside the solenoid, covers 98% of 4π. A typical π^0 mass resolution is 6 MeV. Charged tracks are assigned the most probable mass based on specific ionization, time of flight, and the relative rates for proton, K^+, and π^+ production in B decay.

The undetected neutrino complicates analysis of semileptonic decays. Because of CLEO's hermeticity, we can reconstruct the neutrino via the missing energy ($E_{\text{miss}} \equiv 2E_{\text{beam}} - \sum E_i$) and missing momentum ($\vec{P}_{\text{miss}} \equiv -\sum \vec{p}_i$) in each event. In the process $e^+e^- \to \Upsilon(4S) \to B\bar{B}$, the total energy of the beams is imparted to the $B\bar{B}$ system; at CESR, that system is at rest. The neutrino combined with the signal lepton (ℓ) and meson (m) should thus satisfy the constraints on energy, $\Delta E \equiv (E_\nu + E_\ell + E_m) - E_{\text{beam}} = 0$ and on momentum, $M_{m\ell\nu} \equiv [E_{\text{beam}}^2 - |\vec{p}_\nu + \vec{p}_\ell + \vec{p}_m|^2]^{\frac{1}{2}} = M_B$. Signal Monte Carlo (MC) events have a $|\vec{P}_{\text{miss}}|$ resolution of 110 MeV/c after all cuts. Because the resolution on E_{miss} is about 2.5

times larger [6], we use $(E_\nu, \vec{p}_\nu) = (|\vec{P}_{\text{miss}}|, \vec{P}_{\text{miss}})$ to calculate ΔE and $M_{m\ell\nu}$.

Information from specific ionization is combined with calorimetric and tracking measurements to identify electrons with $p > 600$ MeV/c over 90% of the solid angle. Particles registering hits in counters deeper than five interaction lengths over the polar angle range $|\cos\theta| < 0.85$ are considered muons. Those with hits beyond three interaction lengths over $|\cos\theta| < 0.71$ are used in a multiple-lepton veto, described below. Candidate leptons must have $p_\ell > 1.5$ GeV/c for the π modes and $p_\ell > 2.0$ GeV/c for the ρ and ω (vector) modes, which can couple to the W helicities ±1 and hence have a harder spectrum. The identification efficiency above 1.5 GeV/c averages over 90%; the probability that a hadron is misidentified as a electron (muon), a "fake lepton," is about 0.1% (1%).

A π^0 candidate must have a $\gamma\gamma$ mass within 2 standard deviations of the π^0 mass. We study the ω via its $\pi^+\pi^-\pi^0$ decay; we reduce the combinatoric background by rejecting combinations away from the center of the ω Dalitz plot.

Backgrounds arise from the $e^+e^- \to q\bar{q}$, $\tau^+\tau^-$ continuum, fake leptons, $b \to c\ell\nu$, and other $b \to u\ell\nu$ modes. Continuum backgrounds are reduced tenfold with 70% signal efficiency by comparing the thrust axis of the candidate $m\ell$ pair to that of the other particles. For the signal, the random B daughter orientations determine the axes, while for the jetty continuum, the axes are nearly parallel. We determined the residual continuum background using data collected 60 MeV below the $\Upsilon(4S)$ energy and the fake lepton background by applying measured fake rates to nonleptonic data. The $|p_\ell|$ cuts eliminate background from $b \to c \to s\ell\nu$ and bias against $b \to c\ell\nu$. All criteria were studied with background and signal Monte Carlo, not data, to avoid inducing false signals.

Backgrounds, particularly $b \to c\ell\nu$, can smear into the signal (ΔE, $M_{m\ell\nu}$) region when $\vec{P}_{\text{miss}}$ misrepresents $\vec{p}_\nu$. Such backgrounds are highly suppressed by rejecting events with multiple leptons or a nonzero total charge, indications of missing particles, or with $M_{\text{miss}}^2 \equiv E_{\text{miss}}^2 - |\vec{P}_{\text{miss}}|^2$ inconsistent with zero. Still, Monte Carlo studies show that the dominant remaining $b \to c\ell\nu$ events contain either a K_L or second neutrino (from $c \to s\ell\nu$ with the lepton not identified) roughly colinear with the primary neutrino.

We fit to extract the rates, binning the data in each mode coarsely over the region ($5.1075 \leq M_{m\ell\nu} < 5.2875$ GeV, $|\Delta E| < 0.75$ GeV). The choice of binning balanced separation of signal and background against adequate bin statistics and minimized reliance on detailed MC shape predictions. To examine yields, efficiency, and kinematics, we use the most sensitive bin (the "signal bin") $5.265 \leq M_{m\ell\nu} < 5.2875$ GeV and $-0.15 \leq \Delta E < 0.25$ GeV, though neighboring bins also contribute information to the fit. For comparison, the ΔE and $M_{m\ell\nu}$ resolutions are about 110 and 7.5 MeV, respectively, dominated by the resolution on $|\vec{p}_\nu|$. In the $\rho\ell\nu$ ($\omega\ell\nu$) modes, we further divide the yields into five (four) equal bins over the $\pi\pi$ (3π) mass range within ± 475 MeV (-60 to $+100$ MeV) of the nominal ρ (ω) mass. The 2π (3π) mass interval ± 285 MeV (± 20 MeV) is used for yields and figures for ρ (ω) candidates.

MC simulation provided the distributions in each mode for signal, the $b \rightarrow c$ background, the cross feed among the modes, and the feeddown from higher mass $B \rightarrow H_u\ell\nu$ decays. It included a full description of the $b \rightarrow c$ and charm decay modes and a GEANT-based [7] detector model. The $H_u\ell\nu$ feeddown was evaluated with the ISGW II model [8] for all resonances through the $\rho(1450)$. The observed rate [2] near the lepton-momentum end point fixed the normalization of this component.

We fit the continuum- and fake-subtracted data in the five modes simultaneously. The isospin and quark symmetry relations $\Gamma(B^0 \rightarrow \pi^-\ell^+\nu) = 2\Gamma(B^+ \rightarrow \pi^0\ell^+\nu)$ and $\Gamma(B^0 \rightarrow \rho^-\ell^+\nu) = 2\Gamma(B^+ \rightarrow \rho^0\ell^+\nu) \approx 2\Gamma(B^+ \rightarrow \omega\ell^+\nu)$ constrain the rates for B^+ relative to B^0. Hence we fit for two independent yields, $N_{\pi^\pm}$ and $N_{\rho^\pm}$. Equal charged and neutral B production, $f_{+-} = f_{00}$, is assumed. For self-consistency, the cross feed rates are constrained to the observed yields. The $b \rightarrow c$ normalization in the fit varies independently for each mode. The

normalizations obtained are consistent with that derived from the luminosity and the $\Upsilon(4S)$ production cross section. A typical χ^2 is 145 for 169 degrees of freedom.

We simulate signal and cross feed using several models: ISGW II (a nonrelativistic quark model) [8], three relativistic quark models [9–11], and a hybrid model with a $\pi\ell\nu$ form factor based on dispersion relations [12] and $\rho\ell\nu$ form factors from lattice calculations [13] extended to low q^2 using form factor relations [14,15]. Most model dependence results from variation of efficiency with q^2 induced by the $|p_\ell|$ cuts. The fitted yields (not efficiency corrected) vary with the model because the reconstruction and cross feed probabilities have different q^2 shapes.

In Fig. 1 we show the $M_{m\ell\nu}$ (ΔE) distributions in the ΔE ($M_{m\ell\nu}$) signal band. An excess over background is apparent in both the π and vector meson modes. The lepton momentum spectra for events in the ($M_{m\ell\nu}, \Delta E$) signal bin are also plotted; significant rates beyond 2.4 GeV/c, the approximate $b \rightarrow c\ell\nu$ end point, are clear. Table I lists the data yields, the continuum and fake lepton backgrounds, and the results from the ISGW II fit, all in the signal bin. The $\pi\pi$ (3π) mass distribution for the combined $\rho\ell\nu$ modes ($\omega\ell\nu$ mode) is shown in Fig. 2. A clear excess is observed at the ρ mass. The $\omega\ell\nu$ mode is consistent both with the level expected given the $\rho\ell\nu$ rate and with pure background.

To check for a nonresonant $\pi\pi\ell\nu$ background, we compare these fits to fits with $M_{m\ell\nu}$ and ΔE only for $|m_{\pi\pi} - m_\rho| < 95$ MeV, with and without $\pi\pi$ mass sideband subtraction. The results are consistent with those obtained above, suggesting that the nonresonant contribution is small. We also study $B \rightarrow \pi^0\pi^0\ell\nu$, which can have nonresonant contributions only, and find that the predicted cross feed from the ρ modes is consistent with saturating the observed rate. The bias in the $\rho\ell\nu$ ($\pi\ell\nu$) yield from nonresonant $\pi\pi\ell\nu$ is limited to 20% (5%) by fits that include the $B \rightarrow \pi^0\pi^0\ell\nu$ mode and a nonresonant component generated from an inclusive
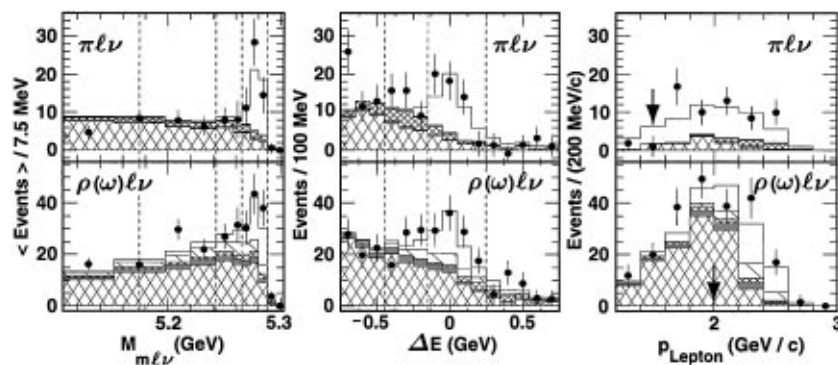

FIG. 1. $M_{m\ell\nu}$ (left), ΔE (center), and $|\vec{p}_\ell|$ (right) in the ΔE and $M_{m\ell\nu}$ signal bands and the signal bin, respectively, for the combined π (top) and vector (bottom) modes. The data (points) are continuum and fake subtracted. The coarse crosshatch, grey, and unshaded compenents are $b \rightarrow cX$, $B \rightarrow H_u\ell\nu$, and signal, respectively. For the π (vector) modes, the fine crosshatch shows vector $\rightarrow \pi$ ($\pi \rightarrow$ vector) and the single hatch, $\pi \rightarrow \pi$ (vector $\rightarrow$ vector) cross feed. Normalizations are from the ISGW II fit. The dashed vertical lines show the binning in the signal bands in the fit. The arrows indicate the $|p_\ell|$ cuts.

TABLE I.   Summary of data yields in the signal bin and the corresponding ISGW II [8] efficiencies and fit results. The errors on the fitted signal yields are completely correlated within the two π modes and within the three vector modes.

	$\pi^{\pm}$	π^0	$\rho^{\pm}$	ρ^0	ω
$\Upsilon(4S)$ yield	46	19	47	73	7
Continuum + fake bkg.	9.8 ± 2.1	1.5 ± 0.5	9.5 ± 2.1	5.8 ± 1.2	0.3 ± 0.8
Efficiency (ISGW II)	0.023	0.015	0.015	0.024	0.006
Signal yield from fit	26.6 ± 6.1	8.6 ± 2.0	19.5 ± 3.3	15.1 ± 2.5	3.5 ± 0.6
$b \to c$ bkg. from fit	7.0 ± 1.2	2.9 ± 0.8	15.2 ± 1.8	21.5 ± 2.2	4.6 ± 1.1
$b \to u$ bkg. in fit	0.5 ± 0.1	0.2 ± 0.1	2.7 ± 0.2	2.9 ± 0.2	0.5 ± 0.1
Cross feed bkg. from fit	4.1 ± 0.8	1.5 ± 0.3	4.9 ± 0.9	13.4 ± 2.5	0.8 ± 0.2

spectator $b \to u\ell\nu$ model and a $\pi\pi$ mass spectrum that is either a ρ lineshape or the dipion shape from a hadronization model.

Table II summarizes the contributions to the systematic errors. Uncertainty in the decay model of the nonsignal B and inaccuracies in detector simulation constitute the dominant contributions. These effects were investigated by varying the K_L^0 fraction, charm semileptonic decay rate, charged particle and photon-finding efficiencies, false charged particle and photon simulation, charged particle momentum resolution, and photon energy resolution. Variations in the rates for $B \to D^{(*)}X\ell\nu$ and for feeddown from higher mass $B \to H_u\ell\nu$ lead to small changes only.

The branching fractions for $B^0 \to \pi^-\ell^+\nu$ and $B^0 \to \rho^-\ell^+\nu$ are listed in Table III for each model. The predicted and observed ρ/π ratios are generally consistent, though the probability that the Körner and Schuler model [10] is consistent is under 0.5%. We choose to exclude this model in averages. The four remaining models give $\mathcal{B}(B^0 \to \pi^+\ell^-\nu) = (1.8 \pm 0.4 \pm 0.3 \pm 0.2) \times 10^{-4}$ and $\mathcal{B}(B^0 \to \rho^+\ell^-\nu) = (2.5 \pm 0.4^{+0.5}_{-0.7} \pm 0.5) \times 10^{-4}$, where the errors are, in order, statistical, systematic, and an estimate of the model uncertainty based on the spread of models and individual model errors. The average ρ/π rate ratio is $1.4^{+0.6}_{-0.4} \pm 0.3 \pm 0.4$.
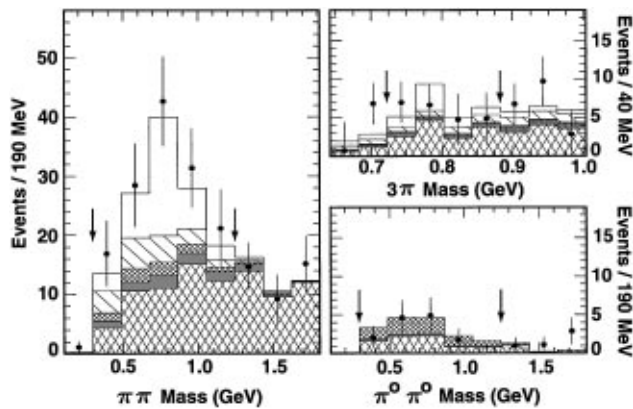
For each model, the branching fractions, isospin relations, and predicted p_ℓ spectral shapes can be combined to obtain a total rate for the five modes into the ranges $2.4 < p_\ell < 2.6$ GeV/c (where π, ρ, and ω should be the dominant modes) and $2.3 < p_\ell < 2.6$ GeV/c (used in the inclusive $|V_{ub}|$ measurements). For the smaller range, we find our rate is consistent with saturation of the inclusive rate measured at CLEO [2], and we obtain the 90% C.L. upper limit of 0.44×10^{-4} on the combined branching fraction of all other modes into this range. For the broader range, we obtain the limit 1.03×10^{-4}.

Table III lists the values extracted for $|V_{ub}|$ from these branching fractions and the predicted partial widths, assuming $\tau_{B^0} = 1.56 \pm 0.05$ ps and $\tau_{B^0}/\tau_{B^+} = 1.02 \pm 0.04$ [16]. To obtain $|V_{ub}|_{\text{avg}}$, the data were refit with the π/ρ ratio fixed to the prediction of each model. Correlations in the modes from our fitting procedure are thereby accounted for; we also account for correlated systematics. Averaging over the the different models, we find $|V_{ub}| = (3.3 \pm 0.2^{+0.3}_{-0.4} \pm 0.7) \times 10^{-3}$, where the errors are statistical, systematic (including B^0 lifetime), and estimated model dependence. This agrees with the value of $|V_{ub}|$ obtained from the inclusive end point rate [2].

These are the first exclusive $b \to u$ branching fraction measurements. The value for $|V_{ub}|$ obtained lends considerable confidence to previously determined values.

FIG. 2.   Reconstructed mass distributions for $\rho \to \pi\pi$ (left), $\omega \to 3\pi$ (top right), and for $\pi^0\pi^0$ from $B \to \pi^0\pi^0\ell\nu$ (bottom right) in the $(M_{m\ell\nu}, \Delta E)$ signal bin. Figure 1 describes the components. The arrows indicate the mass ranges fit.

TABLE II.   Contributions to the systematic error (%) in each branching fraction ($\mathcal{B}$) and the ratio of rates. Simulation of the detector and the second B contribute to ν simulation.

Source	$\mathcal{B}_\pi$	$\mathcal{B}_\rho$	ratio
ν Simulation	14.5	14.8	12.7
$B \to D/D^*X\ell\nu$	2.1	3.2	3.9
Fakes + continuum	5.4	6.7	8.6
$b \to u\ell\nu$ Feeddown	2.2	7.5	9.8
Lepton ID	2.0	2.0	2.0
Luminosity	2.0	2.0	–
$f_{+-}\tau_{+}/f_{00}\tau_0$	3.2	1.9	3.3
Nonresonant $\pi\pi\ell\nu$	-5.0	-20.0	-16.0
Total	$+16.3$	$+18.4$	$+19.0$
	-17.0	-27.2	-24.8

TABLE III.   Final results for each model, with $\Gamma_X \equiv \gamma_X |V_{ub}|^2 \equiv \Gamma(B^0 \to X^- \ell^+ \nu)/10^{12}$ and $\mathcal{B}_X \equiv \mathcal{B}(B^0 \to X^- \ell^+ \nu)$. $\Delta\chi^2$ is the χ^2 change (systematics included) from the best fit to a fit with γ_ρ/γ_π fixed to the prediction. The statistical errors on the ratio are defined by $\Delta\chi^2 = 1$; these errors are highly non-Gaussian. A third error is from estimated form-factor uncertainties.

Model	ISGW II [8]	WSB [9]	KS [10]	Melikhov [11]	Hybrid [12–15]
$\gamma_\rho, \gamma_\pi \ (s^{-1})$	$14.2, 9.6$	$2.1, 7.4$	$33.0, 7.3$	$11.8 \pm 3.4, 7.6 \pm 1.7$	$13.8 \pm 4.0, 13.5 \pm 9.1$
$\mathcal{B}_\pi/10^{-4}$	$2.0 \pm 0.5 \pm 0.3$	$1.8 \pm 0.5 \pm 0.3$	$1.9 \pm 0.5 \pm 0.3$	$1.8 \pm 0.4 \pm 0.3 \pm 0.2$	$1.7 \pm 0.4 \pm 0.3 \pm 0.2$
$\mathcal{B}_\rho/10^{-4}$	$2.2 \pm 0.4^{+0.4}_{-0.6}$	$2.8 \pm 0.5^{+0.5}_{-0.8}$	$1.9 \pm 0.3^{+0.4}_{-0.5}$	$2.8 \pm 0.5^{+0.5}_{-0.8} \pm 0.4$	$2.1 \pm 0.4^{+0.4}_{-0.6} \pm 0.4$
Γ_ρ/Γ_π	$1.1^{+0.5+0.2}_{-0.3-0.3}$	$1.6^{+0.7+0.3}_{-0.5-0.4}$	$1.0^{+0.5+0.2}_{-0.3-0.3}$	$1.6^{+0.7+0.3}_{-0.5-0.4} \pm 0.11$	$1.2^{+0.6+0.2+0.2}_{-0.4-0.3-0.1}$
$\Delta\chi^2$	0.5	3.1	8.1	0.2	0.4
$|V_{ub}|_\pi/10^{-3}$	$3.7 \pm 0.4 \pm 0.3$	$4.0 \pm 0.5 \pm 0.3$	$4.1 \pm 0.5 \pm 0.3$	$3.9 \pm 0.5 \pm 0.3 \pm 0.5$	$2.9 \pm 0.3 \pm 0.2^{+1.3}_{-0.7}$
$|V_{ub}|_\rho/10^{-3}$	$3.2 \pm 0.3^{+0.3}_{-0.4}$	$2.6 \pm 0.2^{+0.2}_{-0.4}$	$2.0 \pm 0.2^{+0.2}_{-0.3}$	$4.0 \pm 0.4^{+0.4}_{-0.5} \pm 0.6$	$3.1 \pm 0.3^{+0.3+0.3}_{-0.4-0.4}$
$|V_{ub}|_{avg}/10^{-3}$	$3.4 \pm 0.2^{+0.3}_{-0.4}$	$2.9 \pm 0.2^{+0.3}_{-0.3}$	$2.2 \pm 0.1^{+0.2}_{-0.3}$	$4.0 \pm 0.2^{+0.35}_{-0.5} \pm 0.5$	$3.1 \pm 0.2^{+0.3}_{-0.4} \pm 0.5$

*Permanent address: BINP, RU-630090 Novosibirsk, Russia.

[1] N. Cabibbo, Phys. Rev. Lett. **10**, 531, (1963); M. Kobayashi and T. Maskawa, Prog. Theor. Phys. **49**, 652 (1973).

[2] R. Fulton *et al.,* Phys. Rev. Lett. **64**, 16 (1990); J. Bartelt *et al.,* Phys. Rev. Lett. **71**, 4111 (1993).

[3] H. Albrecht *et al.,* Phys. Lett. B **234**, 409 (1990); **255**, 297 (1991).

[4] A. Bean *et al.,* Phys. Rev. Lett. **70**, 2681 (1993).

[5] Y. Kubota *et al.,* Nucl. Instrum. Methods Phys. Res., Sect. A **320**, 66 (1992).

[6] Spurious CsI showers from hadronic interactions add linearly to E_{miss}, but tend to average out in the vector sum for $\vec{P}_{miss}$. Incorrect mass assignment also smears E_{miss}.

[7] R. Brun *et al.,* Report No. GEANT 3.15, CERN DD/EE/84-1.

[8] N. Isgur and D. Scora, Phys. Rev. D **52**, 2783 (1995); see also N. Isgur *et al.,* Phys. Rev. D **39**, 799 (1989). The stated errors on the predicted rates are 25% to 50%.

[9] M. Wirbel, B. Stech, and M. Bauer, Z. Phys. C **29**, 637 (1985).

[10] J. G. Körner and G. A. Schuler, Z. Phys. C **38**, 511 (1988).

[11] D. Melikhov, Phys. Rev. D **53**, 2460 (1996); Report No. hep-ph/9603340.

[12] G. Burdman and J. Kambor, FNAL Report No. FERMILAB-Pub-96/033-T, 1996. We take $f_B = 180 \pm 40$ MeV and $g = 0.5 \pm 0.2$.

[13] J. M. Flynn *et al.* (UKQCD), Nucl. Phys. **B461**, 327 (1996); J. M. Flynn *et al.* (UKQCD), Grenada Report No. UG-DFM-3-96, 1996.

[14] B. Stech, Phys. Lett. B **354**, 447 (1995); B. Stech, in Proceedings of the Strasbourg Conference, 1995 (to be published).

[15] We fit UKQCD lattice form factor calculations [13] using the relations $A_0(t)/[1 + \zeta_{A_0}(t)] = V(t)/[1 + \zeta_V(t)] = f_{0V}/(1 - t/m_{0V})^n$ and $A_2(t)/[1 + \zeta_{A_2}(t)] = A_1(t)/\{[1 - t/(m_B^2 + m_\rho^2)^2][1 + \zeta_V(t)]\} = f_{12}/(1 - t/m_{12})^n$, and the constraint $2m_\rho A_0(0) = (m_B + m_\rho)A_1(0) - (m_B - m_\rho) \times A_2(0)$. The $\zeta(t)$ functions are taken from [14]. For $n = 2$, we find $m_{12} = 5.94 \pm 0.17$ GeV, $m_{0V} = 5.42 \pm 0.13$ GeV, and $f_{V0} = 0.36 \pm 0.04$. These parameters and n are varied to explore the uncertainties from the lattice results and our functional form.

[16] I. J. Kroll, FNAL Report No. FERMILAB-CONF-96-032, 1996; in Proceedings of the XVII International Symposium on Lepton-Photon Interactions, Beijing, 1995 (to be published).